Journal of Neuroscience Methods 422 (2025) 110515

Contents lists available at ScienceDirect

Journal of Neuroscience Methods

journal homepage: www.elsevier.com/locate/jneumeth

Primary culture of inner ear schwannoma

Jonas Scheffler [a,*], Arne Liebau [a], Eric Lehner [a], Sandra Leisz [b], Sabine Koitzsch [a], Julia Reiber [a], Anja Harder [c,d], Stefan K. Plontke [a]

[a] Department of Otorhinolaryngology, Head & Neck Surgery, University Medicine Halle, Halle (Saale), Germany
[b] Department of Neurosurgery, University Medicine Halle, Halle (Saale), Germany
[c] CURE-NF Research Group, Medical Faculty, Martin Luther University Halle-Wittenberg, Halle (Saale), Germany
[d] Medical Faculty, University of Muenster, Muenster, Germany

ARTICLE INFO

Keywords:
Inner ear schwannoma
Vestibular schwannoma
Vestibulocochlear schwannoma
Intralabyrinthine schwannoma
Primary culture
Model system
Monocyte infiltration
Cell isolation
Immunofluorescence staining
Semi-automatic quantification

ABSTRACT

Background: Vestibulocochlear schwannomas (VS) are benign tumors arising from Schwann cells of the eighth cranial nerve. While VS are commonly located in the internal auditory canal (IAC) or cerebellopontine angle (CPA), a subset occurs within the inner ear, known as inner ear schwannomas (IES). Their location influences management strategies in terms of tumor control, hearing, and vestibular function. Despite the differences between IES and CPA- or IAC-located VS with respect to epidemiology, anatomical pathology, growth behavior, and clinical management, little is known about biological characteristics of IES.
New method: We developed a reliable technique for isolation of primary tumor cells from ten IES samples for a standardized application. Cells were isolated, processed and cultured for 28 days. Four samples were further characterized by assessing morphology and stability of schwannoma cells as well as presence of monocytic cells.
Results: In all samples, primary cells were successfully cultured and expanded for at least 28 days. Sequential imaging showed characteristic schwannoma cell morphology and a stable growth pattern.
Comparison with existing methods: While existing protocols had focused on establishing primary cultures of VS in the CPA/IAC so far, this study presents the first successful establishment of primary IES cell cultures from different locations within the inner ear.
Conclusion: This work is intended as a proof-of-principle to provide a valuable *in vitro* model system for investigating biological properties of IES, allowing expansion of small samples of a rare schwannoma subtype and *in vitro* analysis of new therapeutic approaches.

1. Introduction

Vestibulocochlear schwannomas (VS) are benign tumors originating from Schwann cells (SC) of the vestibulocochlear nerve and are associated with loss of function of the *NF2*-, *SMARCB1*- or *LZTR*-gene (Plotkin et al., 2022). Most often VS are located in the internal auditory canal (IAC) or in the cerebellopontine angle (CPA) ("classical" VS) (Gupta et al., 2020; Carlson and Link, 2021). VS can also occur in the inner ear and are then called inner ear schwannomas (IES), formerly also named intralabyrinthine schwannoma (ILS) (Plontke et al., 2025). The incidence is described as 1:100.000 in the general population, increasing with age up to 4.1 per 100.000 (Marinelli et al., 2025). The growth rate of IES is usually very slow (Khera et al., 2022; Choudhury et al., 2019). Their specific location in the inner ear and the growth behavior already have implications for the management strategies especially with respect to tumor control, hearing rehabilitation, and - in patients with solely intracochlear IES - for preservation of vestibular receptor function (Iannacone et al., 2024; Plontke et al., 2021, 2025). The epidemiological, anatomical and clinical differences between IES and "classical" VS arouse interest in studying the biological characteristics of IES in more detail. Interestingly, inner ear schwannomas more often arise from the cochlear portion than from the vestibular portion of the eight cranial nerve (Choudhury et al., 2019; Van Abel et al., 2013; Dubernard et al., 2014). Molecular studies of VS have been able to prove the presence of different tumor SC populations. The cellular landscape of schwannomas has specific epigenetic programs and harbors a variety of cell types arising from SC or SC precursors (Liu et al., 2024; Barrett et al., 2024). To date, no data is available on IES, although it is likely that this anatomical location is associated with specific and characteristic Schwannoma cell subtypes. Therefore, methods that allow assessment of

* Correspondence to: Dept. of Otorhinolaryngology, Head and Neck Surgery, University Medicine Halle, Ernst-Grube-Str.40, Halle (Saale) D-06120, Germany.
E-mail address: jonas.scheffler@uk-halle.de (J. Scheffler).

https://doi.org/10.1016/j.jneumeth.2025.110515
Received 12 March 2025; Received in revised form 28 May 2025; Accepted 12 June 2025
Available online 17 June 2025

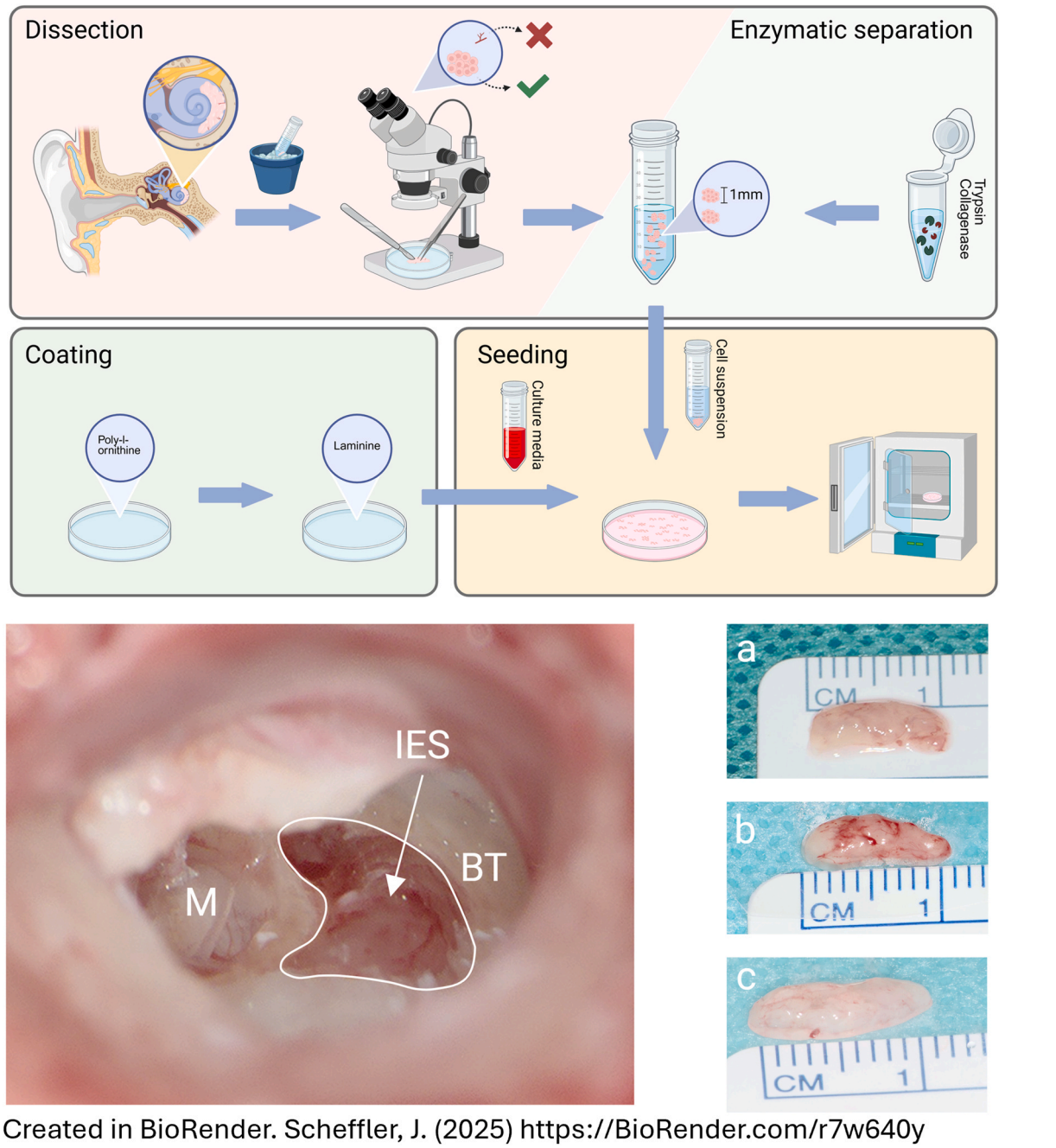

Fig. 1. (up) Schematic representation of the workflow for tumor resection, mechanical/enzymatic sample dissection, preparation of cell culture vessels, and seeding of IES primary cells. (down left) Representative intraoperative view of an IES located within the basal turn of the right cochlea. M, modiolus; BT, basal turn. (down right) a, b, c show representative images of three independent tumor samples after resection with different levels of vascularization. Created in BioRender. Scheffler, J. (2024) BioRender.com/q28i730, (2025) http://BioRender.com/r7w640y.

the molecular biology of schwannoma cells and other tumor cell populations are highly desirable. However, the typically limited sample sizes (compared to CPA- or IAC-located VS) and the usually small numbers of cases even in specialized centers pose a significant challenge to advancing research in this area (Iannacone et al., 2024; Dubernard et al., 2014). Such investigations would provide information not only on schwannoma cell subpopulations but also on metabolic, epigenetic, and immune profiles, progenitor cells, and specific mutation patterns. Obtained data would lead to the development of targeted therapeutic approaches.

In vitro primary cell culture models are a well-established method for the evaluation of tumor growth under controlled environments as well as the analysis of tumor cell morphology and expression patterns on DNA- or protein-level (Dilwali et al., 2014; Xue et al., 2021). As the tumor volume of IES is very small, primary culture of these tumors represents a potent model system, allowing expansion and *in vitro* analysis despite small sample sizes. Although protocols for the cultivation of VS in the CPA or IAC already have been established (Dilwali et al., 2014; Schularick et al., 2014; Leisz et al., 2023), data on successful primary culture of IES are completely missing.

We established primary schwannoma cell culture from IES of different locations within the inner ear (intracochlear, intravestibulocochlear, and transfundal IES with modiolar involvement) and present the first reproducible method to culture primary tumor cells of

surgically resected IES as a potent model system for *in vitro* studies of rare IES.

2. Methods

2.1. Ethics statement

This study was approved by the ethics committee of the Medical Faculty at Martin Luther University Halle-Wittenberg, under process number 2023-231. Written informed consent from patients was obtained prior to sample collection. Samples and clinical data were analyzed anonymously.

2.2. Tumor resection/sample preparation

The following cell separation and culturing procedure was based on and modified from published protocols of VS in the IAC or CPA (Dilwali et al., 2014; Schularick et al., 2014; Landegger et al., 2017). A schematic overview of the experimental workflow is shown in Fig. 1. Tumor samples were collected immediately after surgical tumor removal and photographs of resected tumor samples were taken (Fig. 1). The tumors were cut on a sterile surface and a single solid piece with a size of usually 3–5 × 1–1.5 × 1–1.5 mm for intracochlear tumor samples or a spherical piece of approximately 3 mm for the intravestibular tumor samples was transferred to a sterile 50 ml falcon tube (TPP Techno Plastic Products AG, Trasadingen, Switzerland) containing 20 ml ice-cold buffer-solution with Ca^{2+} and Mg^{2+} (Hanks buffered salt solution HBSS +/+, pH 7.4; or Phosphate-buffered saline PBS, pH 7.4, both ThermoFisher Scientific, Waltham, USA). The tube was placed on ice for further transport. Tumor samples were stored in ice-cold buffer solution for up to 2 h. The next steps were performed under a sterile cell culture hood. The sample was washed 3 times inside the tube with 15 ml ice-cold HBSS -/- (ThermoFisher Scientific, Waltham, USA) or PBS. The sample was then transferred to a sterile, non-coated 10 cm petri dish (TPP Techno Plastic Products AG, Trasadingen, Switzerland), covered with HBSS+/+. Using sterile microsurgical instruments (scalpel, forceps, and scissors) and a surgical microscope, the tumor sample was dissected into smaller pieces of less than 1 × 1 × 1 mm per piece. Any visible blood capillaries were separated from the tumor during this step. Tumor pieces were collected using a 1000 µl pipet (Eppendorf SE, Hamburg, Germany) with a cut-off tip and pipetted into a 15 ml falcon tube (TPP Techno Plastic Products AG, Trasadingen, Switzerland). The falcon tube was centrifuged at 1500 rpm for 3 min. Supernatant was discarded and 500–1000 µl of warm trypsin (0.25 %) and collagenase I (100 U/ml) were added (both ThermoFisher Scientific, Waltham, USA). The falcon tube was placed in the incubator (Heracell VIOS 160i CO2 incubator, ThermoFisher Scientific, Waltham, USA) at 37 °C for 45–60 min. After incubation, 1 ml of cell culture medium (Dulbecco's Modified Eagle's Medium (DMEM) Ham's F12 1:1, 10 % fetal bovine serum (FBS), 1 % Penicillin/Streptomycin, (all purchased from ThermoFisher Scientific, Waltham, USA) was added to stop enzymatic cleavage and the tube was centrifuged at 1500 rpm for 5 min. Supernatant was discarded and the pellet was resuspended 8–10x in cell culture medium using cut-off tips of a 1000 µl pipette. The tips were changed 8–10 times using smaller cut-offs each time. Some smaller cell aggregates usually were unavoidable but did not interfere with successful seeding of cells. Excessive resuspension reduced cell aggregates but eventually resulted in increased cell damage and was therefore avoided. Cell counting using trypan blue dye 0.4 % (NanoEntek, Seoul, Korea) was performed to get an estimation of cell number (Cell Counter NanoEve, NanoEntek, Seoul, Korea). Cells were seeded into cell culture plates/dishes at an estimated concentration of 40.000–80.000 cells/ml.

2.3. Preparation of cell culture vessels

For culturing IES primary cells, coated polycycloalkane- (PCA-) cell culture plates and dishes as well as chamber slides (Sarstedt AG & Co. KG, Nümbrecht, Germany; TPP Techno Plastic Products, Trasadingen, Switzerland) were used. Sterile cell culture vessels were coated with adhesion enhancing synthetic amino acids together with extracellular matrix proteins. Coating the plates with a combination of laminine (20 µg/ml, Sigma Aldrich, Inc., St. Louis, USA) and poly-l-ornithine (0.01 %, Sigma Aldrich, Inc., St. Louis, USA) allowed sufficient adhesion. This coating procedure was performed for standard culture as well as for any imaging- or assay-based experiments. The vessel surface was covered with poly-l-ornithine solution and incubated for 2 h at room temperature (RT) under a sterile cell culture hood. The solution was then discarded and HBSS +/+ containing laminine was added for 2 h at RT. Afterwards, cell culture vessels were washed 1x with HBSS +/+ and prepared for further use.

2.4. Cell culture procedure, passaging and cryoconservation

For seeding and culturing IES primary cells, DMEM/F12 with 10 % FBS and 1 % Penicillin/Streptomycin (all from ThermoFisher Scientific, Waltham, USA) was used as cell culture medium. All culture dishes used for culturing IES primary cells were PCA-based and coated with poly-l-ornithine and laminine as described above. After seeding, the plates were placed in the incubator at 37 °C and 5 % CO_2. The cells stayed untouched in the incubator for at least 48 h prior to the first cell culture medium change. Adhesion of cells usually occurred during the first 24 h after seeding. When seeding 40.000–80.000 cells/ml in 6-well format cell culture plates (TPP Techno Plastic Products AG, Trasadingen, Switzerland), cell culture medium containing phenol red usually indicated change of pH-value after 48–72 h. Primary IES cells were cultured for at least 28 d under the conditions stated above. Detaching and passaging of cells into fresh cell culture plates is possible, once confluence is reached, but not obligatory for retaining cell viability. Passaging was performed by incubation of primary IES cells with trypsin 0.05 % (ThermoFisher Scientific, Waltham, USA) for 6 min. Enzymatic reaction was stopped by adding culture medium containing 10 % FBS and repeated resuspension. Cells were transferred to a 15 ml falcon tube and centrifuged at 1000 rpm for 5 min. After resuspending cells in fresh culture media, they were transferred to freshly coated cell culture dishes. Cell culture medium was changed every 48–72 h depending on indicated medium toxicity. Cryopreservation of primary IES cells was performed by using 10 % Dimethyl Sulfoxide (DMSO, Sigma-Aldrich, Inc., St. Louis, USA in DMEM F12 with 20 % FBS. Human primary fibroblasts (hFB25-cells) derived from human conjunctiva were cultured under the exact same conditions as a control. These cells were kindly provided by Joana Heinzelmann, University Medicine Halle, Department of Ophthalmology.

2.5. Immunofluorescence staining and microscopy

Immunofluorescent staining and microscopy were performed on coated PCA-cell culture chamber slides after culturing primary IES cells for 7 d, 14 d, and 28 d. Cell culture medium was discarded, and slides were washed 3x with PBS. Cells were fixed with 4 % paraformaldehyde (PFA) in PBS for 10 min at RT. Fixation solution was immediately removed and cells were washed 1x with ice-cold PBS. Gentle permeabilization was achieved by adding 0.5 % saponin (Sigma-Aldrich, Inc., St. Louis, USA), in PBS-T (PBS containing 0.1 % Tween 20, Sigma-Aldrich, Inc., St. Louis, USA) for another 10 min. Cells were washed 3x for 5 min with cold 0.05 % saponin in PBS-T. The cells were then incubated with blocking solution (1 % bovine serum albumin (BSA), Sigma-Aldrich, Inc., St. Louis, USA, 0.05 % saponin in PBS-T) for 30 min. Afterwards, cells were incubated with primary antibody solution (S100 Beta Rabbit Polyclonal antibody and cluster of differentiation 68 (CD68) Mouse Monoclonal antibody, Proteintech, Rosemont, USA) in 1 % BSA, 0.05 % saponin in PBS-T for at least 1 h at RT. The solution was removed, and cells were washed 3x for 5 min with 0.05 % saponin in

Table 1
Clinical features and tumor classification of IES1-4.

Patient number	m/f	Age at surgery	Duration between first clinical symptom likely associated with IES and surgery (in years)	Tumor classification (Plontke et al., 2025)	Sample location
IES1	f	64	6	intracochlear	intracochlear
IES2	m	63	13	intravestibulocochlear and transfundal with modiolar involvement	intravestibular
IES3	m	57	1	intracochlear	intracochlear
IES4	f	23	3	intravestibulocochlear	intracochlear

PBS-T. Secondary antibody solution (CoraLite488-conjugated Goat Anti-Rabbit IgG; CoraLite647-conjugated Goat Anti-Mouse IgG, Proteintech, Rosemont, USA) in 1 % BSA, 0.05 % saponin in PBS-T was added for 2 h at RT in the dark. Cells were washed 3 times for 5 min with 0.05 % saponin in PBS-T. Solution was discarded, chamber walls were lifted from the chamber slide and mountant dying solution containing 4′,6-Diamidino-2-phenylindol (DAPI) dye (ThermoFisher Scientific, Waltham, USA) was added to the slide surface followed by coverslips. The slides were protected from light until transferred for microscopy. Fluorescent images were taken using Nikon ECLIPSE Ti2-E fluorescence microscope (Nikon, Tokio, Japan). Excitation wavelength for DAPI channel was 375 nm, for near-infrared fluorescent protein (IRFP) channel 620 nm, and for green fluorescent protein (GFP) channel 480 nm. Channeled images were taken at 10x or 40x magnification. The separate channels were later merged using the software NIS-Elements (Nikon, Tokio, Japan). For each chamber, at least 10 independent images were taken.

2.6. Fluorescence image analysis, cell counting and cell proliferation, flow-cytometry analysis

Quantitative analysis of fluorescence images and cell counting were performed using semi-automatic object-based colocalization for ImageJ (Version 1.54f) (Lunde and Glover, 2020). Multichannel grayscale and binary images were created using the Colocalization Image Creator PlugIn. Upper and lower thresholds of binary images were set to exclude artifacts and background noise. A grayscale image overlay was used to visually control object identification. Identified and colocalized objects were automatically quantified using the Colocalization Object Counter. Identification settings were saved and verified or adapted manually, if necessary. Colocalization of GFP and DAPI fluorescent channel was rated as a S100B-positive, DAPI-positive object. Separate localization of DAPI fluorescent signal was rated as a S100B-negative, DAPI-positive object. Cells showing a weak positive signal for Protein S100B that was below the automatic detection threshold were not counted as Protein S100B-positive cells in the semi-quantitative image analysis. Red

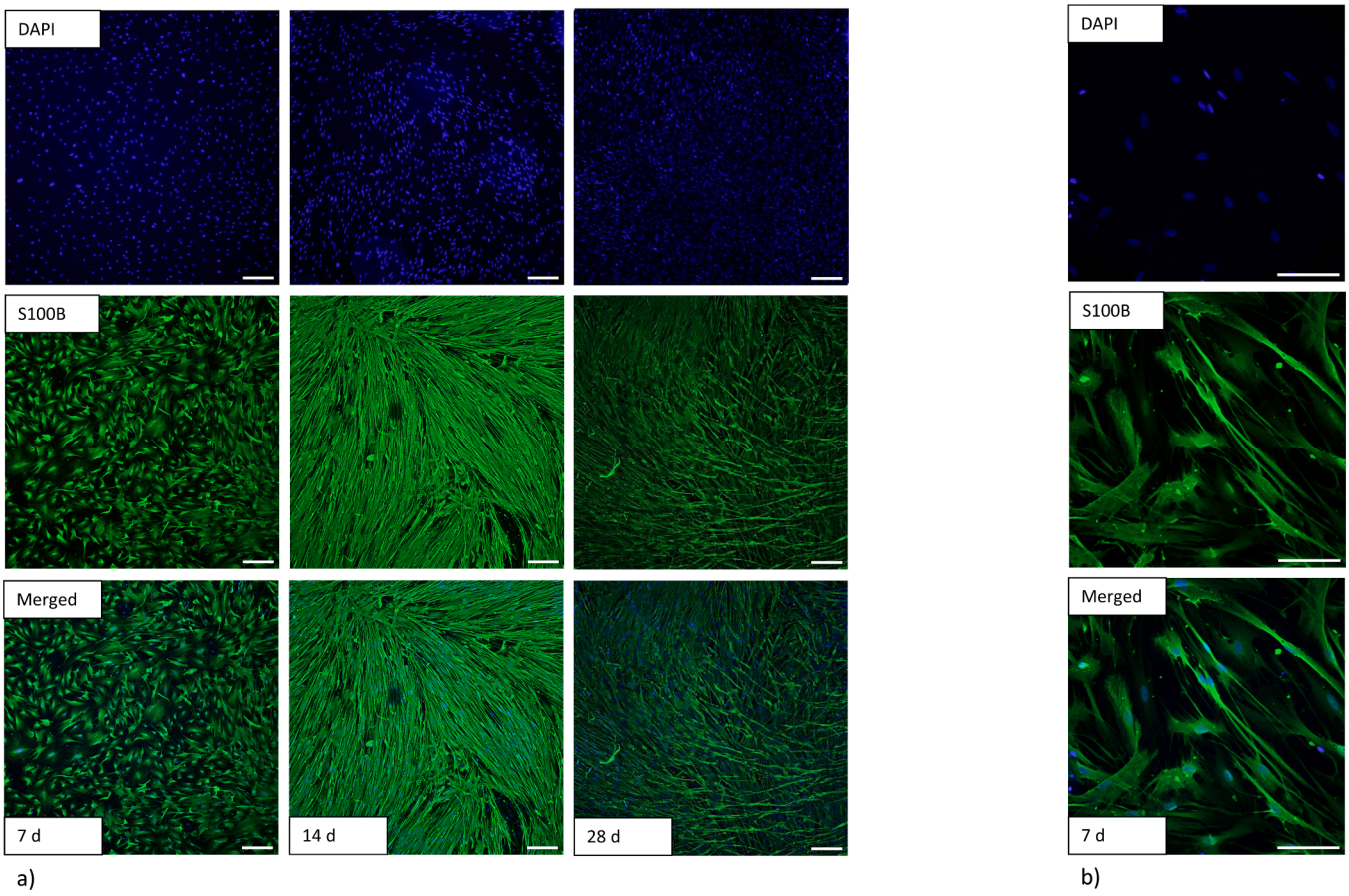

Fig. 2. Representative immunofluorescent images of coverslides with IES primary cultures. Cells were fixed and staining was performed with primary antibody against intracellular/ intranuclear S100B as a schwannoma cell marker and conjugated secondary antibody (green channel, mid row) together with DAPI dye for staining of nuclei (blue channel, top row). Merged channels in the bottom row. a) Primary cultures of IES3 after 7°d, 14°d and 28°d. 10x magnification, white scalebars represent 200°µm. b) Primary cultures of IES4 after 7°d. 40x magnification, white scalebars represent 100°µm.

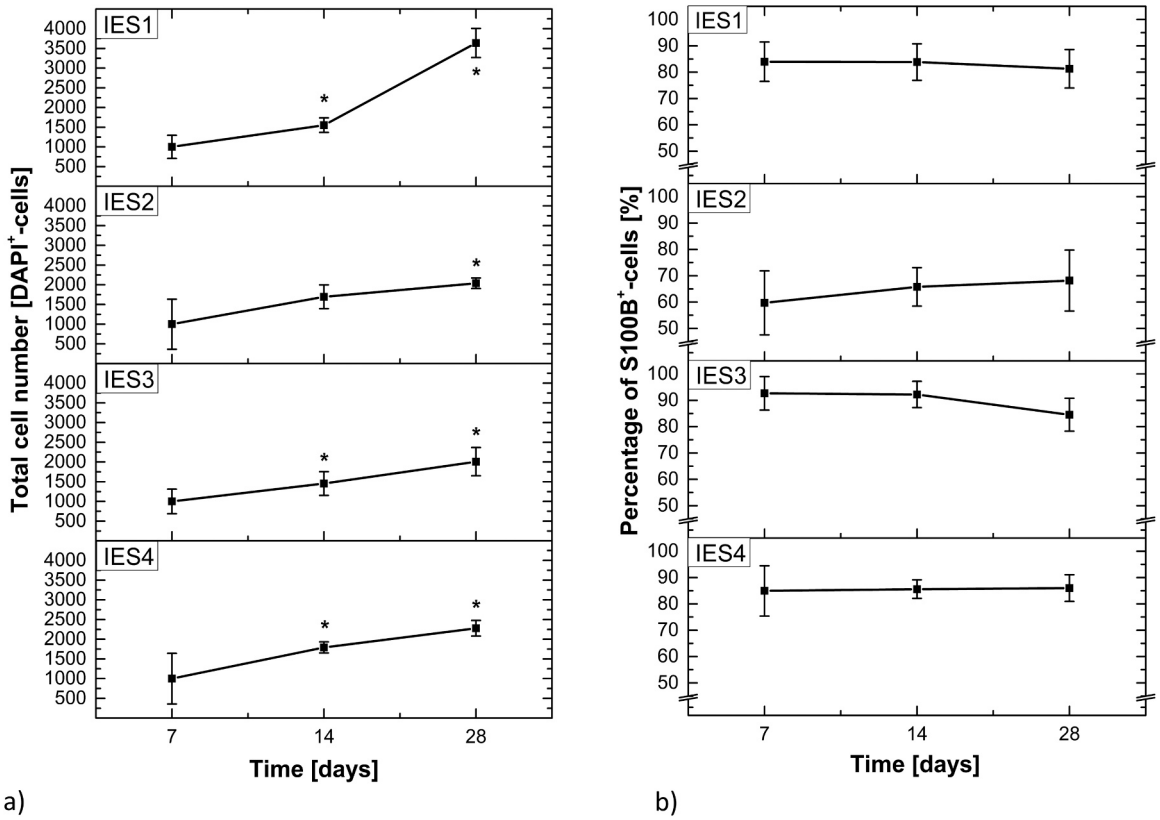

Fig. 3. Quantitative analysis of immunofluorescent images of IES primary cells using semi-automatic object-based colocalization PlugIn for ImageJ. Each row represents one tumor specimen: IES1-intracochlear, IES2-transfundal with modiolar involvement, IES3-intracochlear, IES4-intravestibulocochlear. a) Single positive $DAPI^+$-signals (single stained nuclei) were interpreted as singular cells. Cells were counted after primary culture for 7 d, 14 d, and 28 d. Graph shows mean values and standard deviations from 10 independent images per sample and per timepoint. b) Amount of $S100B^+/DAPI^+$-signals, which were interpreted as schwannoma cells, in relation to total cell number ($S100B^{+/-}/DAPI^+$-cells). Graph shows mean values and standard deviation from 10 independent images per sample and per timepoint. * indicates a p-value < 0.05.

fluorescent protein (RFP) fluorescent signal in colocalization with DAPI fluorescent signal was rated as CD68-positive. Minimum radius for detection of objects was set as 5 pixels. Cell count per experiment was estimated by calculating the mean object count and standard deviation of 10 random images. Increase of cell number as a surrogate marker for proliferation per culture was assessed by sequential cell counting after 7 d, 14 d, and 28 d calculating the increase in mean cell counts from 10 random immunofluorescent pictures. To investigate the relative amount of fibroblasts, three independent IES primary culture samples (cultured for 21–28 d) were admitted to flow cytometry analysis after staining cells with CD90-antibody according to the manufacturer's instructions (FITC Anti-CD90 / Thy1 antibody [F15-42-1], abcam 11155, abcam, Cambridge, UK). HFB25-cells were used as a positive control. Unstained cells were used as a negative control.

2.7. Quantification of IES metabolic activity

To verify the results of semi-automatic quantification via fluorescence microscopy, metabolic activity of IES cells at different time points was assessed using tetrazolium salt (MTS) assay (CellTiter 96® AQ_{ueous} One Solution Cell Proliferation Assay, Promega, Madison, USA). Cells were cultured under the above stated conditions in a 96-well plate format (TPP Techno Plastic Products AG, Trasadingen, Switzerland). After 7 d, 14 d, and 21 d, cell culture medium containing MTS reagent was added to IES cells. Absorbance at 490 nm was measured after 1 h incubation time using a fluorescence spectrophotometer (Cytation 5, Agilent Technologies, Inc., Santa Clara, USA). HFB25-cells were cultured under similar conditions as a fibroblast control and metabolic activity was assessed after 3 d and 7 d. Absorbance was measured at 490 nm after 1 h incubation time.

3. Results

Tumor samples from ten patients with IES were collected and cells were isolated as described above (Fig. 1). Four samples were further characterized as described in this work. Tumors from patients #1 and #3 were intracochlear IES, the tumor from patient #2 was a transfundal IES with modiolar involvement, and the tumor from patient #4 was an intravestibulocochlear IES (Table 1). While macroscopically appearing similar in colour and texture, vascularization differed between different tumor samples (Fig. 1). In all 10 samples, viable cells could be extracted and cultured for at least 28 d. Immunofluorescent staining revealed typical schwannoma cell morphology of elongated spindle cells with bipolar processes. All cultures showed strong positive staining for S100B as an established SC marker (Fig. 2). The increase in cell number over time as determined by sequential counting of DAPI-positive cells is shown in Fig. 3a. Fig. 3b shows the amount of $S100B^+/DAPI^+$-cells in relation to $S100B^{+/-}$/ $DAPI^+$-cells. The percentage of $S100B^+$- cells differed between the samples, with IES3 showing the lowest relative amount of schwannoma cells (about 65 %), while in the other samples it was between 80 % and 90 %. The percentage of $S100B^+$/ $DAPI^+$-cells (schwannoma cells) remained stable over the timespan of 28 d. Using immunofluorescence imaging, $S100B^+$- cells reflected the same morphology and growth as seen conventionally: Schwannoma cells demonstrated a spindle-like, bipolar shape and a longitudinal growth (Dilwali et al., 2014; Schularick et al., 2014). Cells tended to arrange in a parallel manner during the first 2–3 weeks of culture. After that, a more disorganized growth of $S100B^+$- cellular processes was noticed. One

Figure 4

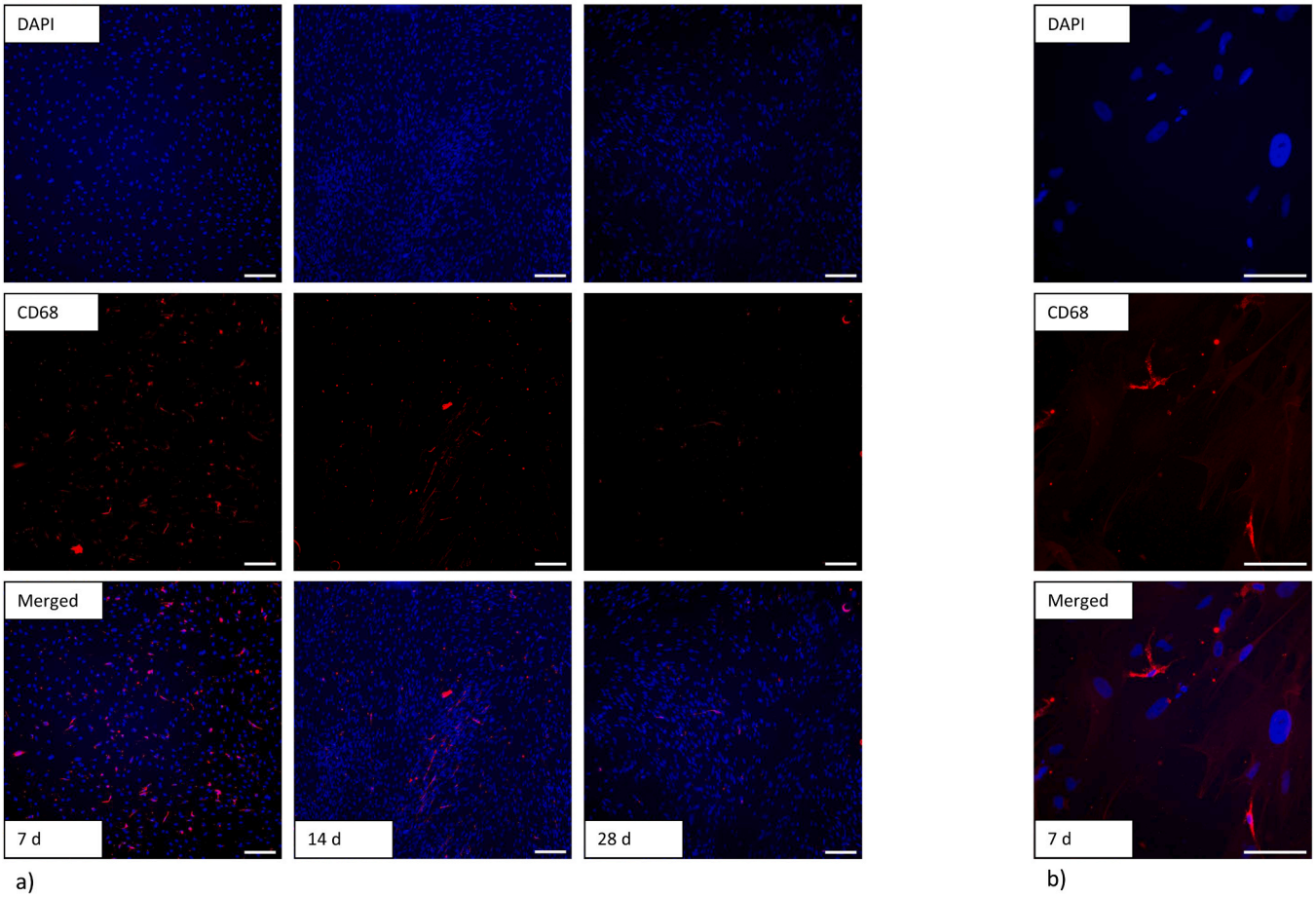

Fig. 4. Representative immunofluorescent images of coverslides with IES primary cultures. Cells were fixed and staining was performed with primary antibody against monocytic marker CD68 and conjugated secondary antibody (RFP channel) together with DAPI dye for staining of nuclei (DAPI channel). a) Primary cultures of IES3 after 7°d, 14°d and 28°d. 10x magnification, white scalebars represent 200°µm. b) Primary cultures of IES2 after 7°d. 40x magnification, white scalebars represent 100°µm.

sample was cultured for 3 months to explore long-term stability and lifespan in culture (Supplementary figure S1). Schwannoma cells displayed similar growth patterns, independent of the location within the inner ear.

Sequential staining for CD68 as a marker for monocytes indicated a proximity of $CD68^+$-cells to $S100B^+$-cells. CD68-positive cells generated multiple processes (Fig. 4). IES from patient #2 showed the highest ratio of $CD68^+$-cells with about 7 % after 7 d and 14 d of culture. After 28 d of culture, the number of $CD68^+$-cells declined to <2 %. Analysis of tumors from patients #3 and #4 showed a ratio of <2 % of $CD68^+$-cells at all timepoints without any significant change over time (Fig. 5).

In order to estimate the relative amount of tumor associated fibroblasts and to rule out excessive fibroblast-induced contamination, flow cytometry analysis of three independent IES samples were performed after 21 d–28 d of culture. The cells were stained for CD90 as an established fibroblast marker. HFB25-cells were used as a positive control. The relative amount of CD90-positive cells was 0.9 %, 6.3 % and 38 %, respectively.

Results of semi-automatic quantification via fluorescence microscopy were verified by performing MTS assays at different time points. Absorbance values of cell culture medium after incubation of cells with MTS correlated with metabolic activity of corresponding cells and were interpreted as an indirect measure for cell viability and number. (Correlation of absorbance values with cell numbers of semi-automatic counting is shown in supplementary figure S2). Comparative MTS-assay analysis differed between IES cultures and hFB25-cells. Fibroblasts reached confluence of >90 % after 7d and absorbance values exceeded those of IES primary cells cultured under the same conditions (Supplementary figure S2).

4. Discussion

Although various reports have addressed different *in vitro* model systems of "classic" VS (i.e., in the IAC or CPA) (Dilwali et al., 2014; Schularick et al., 2014; Leisz et al., 2023), limitations must be considered when establishing *in vitro* models of IES. IES have a distinctly smaller tumor mass and differ in their surrounding milieu as they are commonly located within the perilymph space. Contact to the endolymphatic space seems likely due to frequent tumor extension to the osseus basilar lamina described in a histopathological study (Bagattini et al., 2021). Intraoperative observations frequently show physical contact between tumor mass and the endolymphatic space. Both the endolymphatic and perilymphatic space are separated from the vascular system and blood by membraneous barriers. This hints towards a distinct composition of surrounding fluids of IES (Salt and Hirose, 2018; Thalmann et al., 1994; Leary Swan et al., 2009). Although the vascularization characteristics of IES tissue are still unknown, the blood-labyrinthine barrier likely complicates a potential systemic drug therapy. However, IES might be approached with local treatment due to their location within the fluid-filled cavities of the cochlear scale, which are accessible through its membranous boundaries to the middle ear.

IES not only differ from VS in the IAC/CPA and schwannomas in

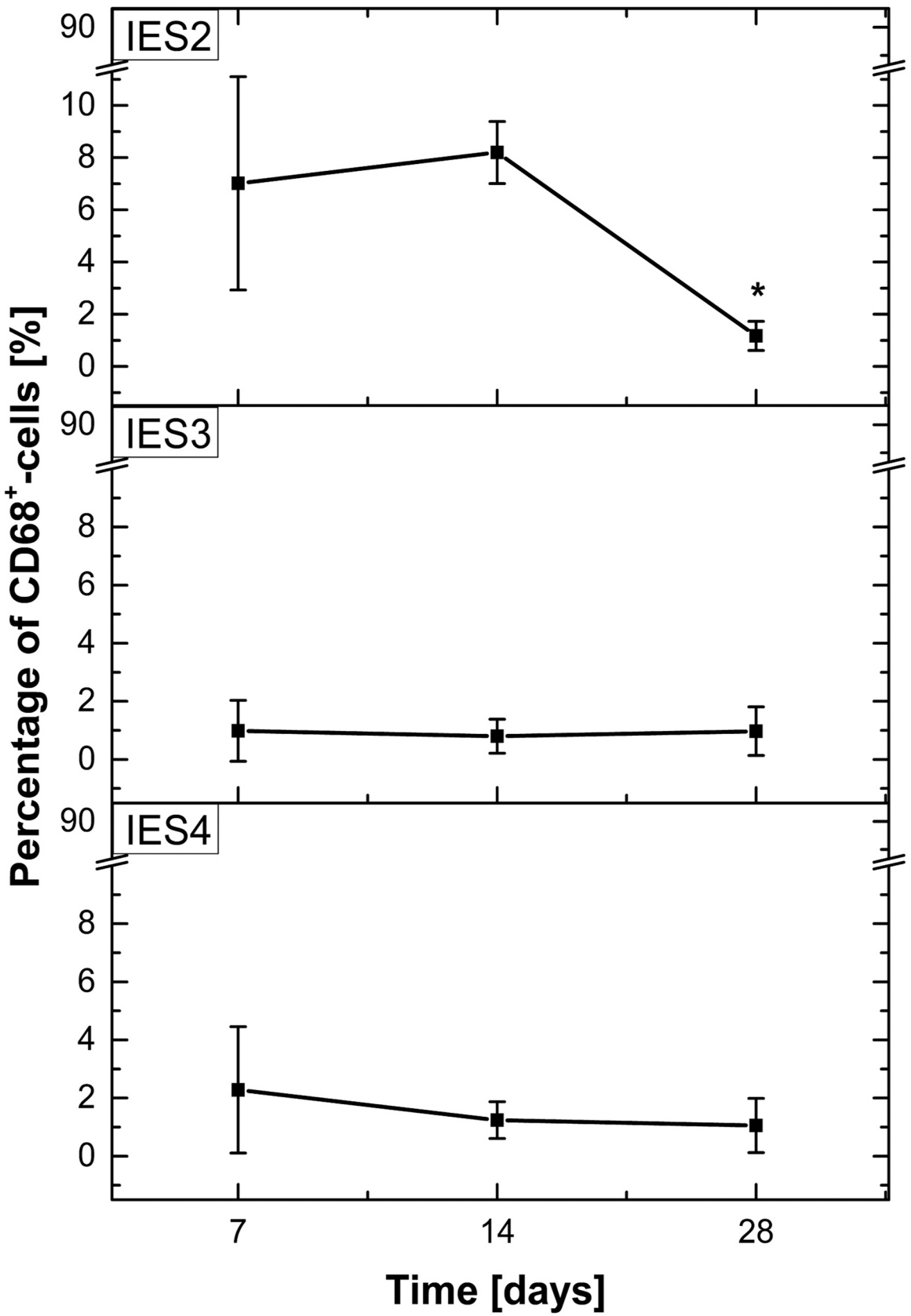

Fig. 5. Quantitative analysis of immunofluorescent images of IES primary cells using semi-automatic object-based colocalization PlugIn for ImageJ. Each row represents one tumor specimen: IES2-transfundal with modiolar involvement, IES3-intracochlear, IES4-intravestibulocochlear. The graph shows the amount of $CD68^{+}/DAPI^{+}$-cells in relation to total cell number ($CD68^{+/-}/DAPI^{+}$-cells). Displayed are the mean values and standard deviations from 10 independent images per sample and per timepoint.* indicates a p-value < 0.05.

other locations in the human body with respect to growth and location: Histological studies of IES did not show any cystic transformation, a phenomenon that is frequently observed in "classic" VS. Additionally, IES are located in a completely different microenvironment compared to other schwannoma locations along the vestibulocochlear nerve (Bagattini et al., 2021; Gomez-Brouchet et al., 2001). Immunohistochemical studies of IES tumor slices in the literature have yet been limited to classical SC markers like protein S100B (Plontke et al., 2017).

Many features of this tumor type are unresolved and make a model system urgently necessary. Reproducible *in vitro* models of IES will help to address more than morphological features of IES and to evaluate effects of new therapeutic agents on a cellular level. Here, we were able to establish the first reproducible protocol for primary culture of different types of IES. All samples showed a strong signal for S100B, indicating the predominant presence of schwannoma cells (Schularick et al., 2014). IES usually grow very slowly *in vivo*, which was also reflected in the slow increase in cell number of IES cells in the primary culture. Nevertheless, it was possible to expand the primary culture while retaining a stable amount of schwannoma cells, allowing multiple analyses from singular small tumor samples. We verified the results from semiquantitative cell counting by performing MTS metabolic activity assay. MTS-assay might therefore be used as an easy and quick alternative for estimation of cell proliferation of IES. Subsequent immunofluorescent staining of S100B showed a consistent ratio of schwannoma cells within the cultures after 7 d, 14 d, and 28 d. This suggests stability of the primary culture over a timespan of at least 28 d, thus allowing long-term *in vitro* studies of cell morphology and testing of therapeutic agents.

Myeloic cells are known to be present in schwannomas. In our model, $CD68^+$-monocytes occurred with different frequencies in tumor samples (Hannan et al., 2020). In the culture of IES cells from patient #2, the initial ratio of monocytic cells was about 3 times higher than in the other samples, hinting towards a relevant infiltration of IES tissue with tumor associated monocytes/macrophages. Notable in the clinical data of patient #2 is the complex intravestibulocochlear, transfundal tumor growth with modiolar involvement, as well as the duration of 13 years between onset of symptoms and surgery (Table 1). A connection between monocyte invasion and tumor complexity or disease progression in IES might thus be possible and an interesting objective of future studies. Subsequent immunofluorescent imaging over the timespan of 28 d showed a decline of $CD68^+$ cells. Conceivable causes for the low amount of $CD68^+$ cells in cultures of tumor cells from patients #3 and #4 as well as the decline of $CD68^+$ cells in tumor cells from patients #2 could be a loss of tumor associated immune cells during the mechanical and enzymatic processing of tumor samples, changes in the inflammatory microenvironment as well as senescence of these cells during culture. Our findings suggest the first two weeks of primary culture as feasible for investigating tumor associated monocytes/macrophages.

Fibroblast contamination is a common phenomenon in primary tumor cell cultures. In our experiments, sequential staining showed no significant reduction in the proportion of S100B-positive cells over 28 d, suggesting no substantial overgrowth by other cell types, such as rapidly proliferating fibroblasts. To further validate these findings, we performed flow cytometry analysis on three independent cryopreserved IES samples cultured 21–28 d. Cells were stained for CD90, a well-established fibroblast marker, and the proportion of CD90-positive cells was compared to that in human primary fibroblasts (hFB25-cells), which served as a positive control (99.7 % CD90-positive). The IES samples showed 0.9 %, 6.3 %, and 38.6 % CD90-positive cells, respectively (Supplementary figure S3). While indicating culture stability for 28 d, these findings also hint towards a possible influence of other IES-associated cellular subtypes, such as tumor-associated fibroblasts, on the morphology of IES.

In conclusion, we report the first successful and reproducible protocol for primary culture of IES. This work represents a proof-of-principle that IES can be modeled *in vitro*. This important step clearly expands the spectrum of molecular studies for prognostic and diagnostic purposes to develop new, e.g. pharmacological therapeutic strategies for IES.

CRediT authorship contribution statement

Jonas Scheffler: Writing – original draft, Visualization, Software, Resources, Project administration, Methodology, Investigation, Formal analysis, Data curation, Conceptualization. **Arne Liebau:** Writing – review & editing, Validation, Supervision, Methodology. **Eric Lehner:** Writing – original draft, Validation, Software, Methodology, Data curation. **Sandra Leisz:** Writing – original draft, Validation, Methodology. **Stefan K. Plontke:** Writing – original draft, Supervision, Project administration, Methodology, Investigation, Conceptualization. **Sabine Koitzsch:** Resources, Project administration, Methodology. **Julia Reiber:** Writing – original draft, Visualization, Validation, Software. **Anja Harder:** Writing – original draft, Supervision.

Declaration of Competing Interest

Disclosures are described under in the submitted individual author disclosure forms. The institution of SKP, JS, AL, SK, JR, and EL receive research support from Cochlear Ltd., Sydney Australia, and MED-EL, Innsbruck, Austria for projects not related to this work. No extramural funding was required for this project.

Acknowledgements

The authors would like to thank Dr. Joana Heinzelmann, Department of Ophthalmology, University Medicine Halle, for kindly providing human primary fibroblasts for this study. They also thank Dr. Alexander Navarrete-Santos and Annika Weißenborn from the FACS Core Facility, University Medicine Halle, for their support with the flow cytometry analysis.

Supporting information

Supplementary figure S1: Representative immunofluorescent image of a coverslide with primary culture of IES3 after 84 d. 10x magnification. Cells were fixed and staining was performed with primary antibody against intracellular/ intranuclear S100B and conjugated secondary antibody (GFP channel) together with DAPI dye for staining nuclei (DAPI channel). Images of multiple z-levels had to be stacked and focused, as cells tended to form a cone-like, three-dimensional structure.

Supplementary figure S2: Comparison of MTS metabolic assay and cell counting via quantitative analysis of immunofluorescent images. IES cells were cultured for 7 d, 14 d, 21 d. The full line shows means and standard deviations of absorbance values at 490 nm measured with a fluorospectrometer after incubation of IES cells with MTS-reagent for 1 h. The dashed line shows IES cell mean number and standard deviation calculated by semi-automatic object-based colocalization PlugIn for ImageJ. HFB25-cells were cultured under similar conditions and comparative MTS metabolic assay was performed after 3 d and 7 d. For each method two independent tumor samples were analysed ($n = 2$). * indicates a p-value < 0.05.

Supplementary figure S3: Flow cytometry analysis of three independent samples of IES primary culture (cells were cultured for 21–28 d) after staining for CD90. HFB25-cells are fibroblasts and were used as positive control. P6 indicates relative amount of CD90-positive signals.

Appendix A. Supporting information

Supplementary data associated with this article can be found in the online version at doi:10.1016/j.jneumeth.2025.110515.

Data availability

Data will be made available on request.

References

Bagattini, M., Quesnel, A.M., Röösli, C., 2021. Histopathologic evaluation of intralabyrinthine schwannoma. Audiol. Neurotol. 26 (4), 265–272. https://doi.org/10.1159/000511634.

Barrett, T.F., Patel, B., Khan, S.M., et al., 2024. Single-cell multi-omic analysis of the vestibular schwannoma ecosystem uncovers a nerve injury-like state. Nat. Commun. 15 (1), 478. https://doi.org/10.1038/s41467-023-42762-w.

Carlson, M.L., Link, M.J., 2021. Vestibular schwannomas. N. Engl. J. Med. 384 (14), 1335–1348. https://doi.org/10.1056/NEJMra2020394 (Ingelfinger JR, ed.

Choudhury, B., Carlson, M.L., Jethanamest, D., 2019. Intralabyrinthine schwannomas: disease presentation, tumor management, and hearing rehabilitation. J. Neurol. Surg. B Skull Base 80 (2), 196–202. https://doi.org/10.1055/s-0039-1678731.

Dilwali, S., Patel, P.B., Roberts, D.S., et al., 2014. Primary culture of human Schwann and schwannoma cells: improved and simplified protocol. Hear. Res. 315, 25–33. https://doi.org/10.1016/j.heares.2014.05.006.

Dilwali, S., Patel, P.B., Roberts, D.S., et al., 2014. Primary culture of human Schwann and schwannoma cells: improved and simplified protocol. Hear. Res. 315, 25–33. https://doi.org/10.1016/j.heares.2014.05.006.

Dubernard, X., Somers, T., Veros, K., et al., 2014. Clinical presentation of intralabyrinthine schwannomas: a multicenter study of 110 cases. Otol. Neurotol. 35. ⟨http://journals.lww.com/otology-neurotology⟩.

Gomez-Brouchet, A., Delisle, M.B., Cognard, C., et al., 2001. Vestibular schwannomas: correlations between magnetic resonance imaging and histopathologic appearance. Otol. Neurotol. ⟨http://journals.lww.com/otology-neurotology⟩.

Gupta, V.K., Thakker, A., Gupta, K.K., 2020. Vestibular schwannoma: what we know and where we are heading. Head Neck Pathol. 14 (4), 1058–1066. https://doi.org/10.1007/s12105-020-01155-x.

Hannan, C.J., Lewis, D., O'Leary, C., et al., 2020. The inflammatory microenvironment in vestibular schwannoma. Neurooncol. Adv. 2 (1). https://doi.org/10.1093/noajnl/vdaa023.

Iannacone, F.P., Rahne, T., Zanoletti, E., Plontke, S.K., 2024. Cochlear implantation in patients with inner ear schwannomas: a systematic review and meta-analysis of audiological outcomes. Eur. Arch. Oto-Rhino-Laryngol. https://doi.org/10.1007/s00405-024-08818-3.

Khera, Z., Kay-Rivest, E., Friedmann, D.R., Mcmenomey, S.O., Thomas Roland, J., Jethanamest, D., 2022. The natural history of primary inner ear schwannomas: outcomes of long-term follow-up. Otol. Neurotol. 43 (10), E1168–E1173. https://doi.org/10.1097/MAO.0000000000003698.

Landegger, L.D., Sagers, J.E., Dilwali, S., Fujita, T., Sahin, M.I., Stankovic, K.M., 2017. A unified methodological framework for vestibular schwannoma research. J. Vis. Exp. (124). https://doi.org/10.3791/55827.

Leary Swan, E.E., Peppi, M., Chen, Z., et al., 2009. Proteomics analysis of perilymph and cerebrospinal fluid in mouse. Laryngoscope 119 (5), 953–958. https://doi.org/10.1002/lary.20209.

Leisz, S., Klause, C.H., Becker, A.L., et al., 2023. Establishment of vestibular schwannoma primary cell cultures obtained from cavitron ultrasonic surgical aspirator tissue material. J. Neurosci. Methods 397. https://doi.org/10.1016/j.jneumeth.2023.109955.

Liu, S.J., Casey-Clyde, T., Cho, N.W., et al., 2024. Epigenetic reprogramming shapes the cellular landscape of schwannoma. Nat. Commun. 15 (1), 476. https://doi.org/10.1038/s41467-023-40408-5.

Lunde, A., Glover, J.C., 2020. A versatile toolbox for semi-automatic cell-by-cell object-based colocalization analysis. Sci. Rep. 10 (1). https://doi.org/10.1038/s41598-020-75835-7.

Marinelli, J.P., Rahne, T., Dornhoffer, J.R., et al., 2025. Cochlear implantation with sporadic inner ear schwannomas: outcomes in 106 patients from an international multi-institutional study. Otol. Neurotol. 46 (1), 10–18. https://doi.org/10.1097/MAO.0000000000004362.

Plontke, S.K., Lloyd, S.K.W., Freeman, S.R.M., et al., 2025. Revised classification of inner ear schwannomas. Otol. Neurotol. In press.

Plontke, S.K., Rahne, T., Pfister, M., et al., 2017. Intralabyrinthine schwannomas: surgical management and hearing rehabilitation with cochlear implants. HNO 65, 136–148. https://doi.org/10.1007/s00106-017-0364-6.

Plontke, S.K., Rahne, T., Curthoys, I.S., Håkansson, B., Fröhlich, L., 2021. A case series shows independent vestibular labyrinthine function after major surgical trauma to the human cochlea. Commun. Med. 1 (1). https://doi.org/10.1038/s43856-021-00036-w.

Plontke, S.K., Lloyd, S.K.W., Freeman, S.R.M., et al., 2025. Revised Classification of Inner Ear Schwannomas. Otol. Neurotol. 46 (1), 3–9. https://doi.org/10.1097/MAO.0000000000004363. Epub 2024 Oct 28. PMID: 39473303.

Plotkin, S.R., Messiaen, L., Legius, E., et al., 2022. Updated diagnostic criteria and nomenclature for neurofibromatosis type 2 and schwannomatosis: an international consensus recommendation. Genet. Med. 24 (9), 1967–1977. https://doi.org/10.1016/j.gim.2022.05.007.

Salt, A.N., Hirose, K., 2018. Communication pathways to and from the inner ear and their contributions to drug delivery. Hear. Res. 362, 25–37. https://doi.org/10.1016/j.heares.2017.12.010.

Schularick, N.M., Clark, J.J., Hansen, M.R., 2014. Primary culture of human vestibular schwannomas. J. Vis. Exp. (89). https://doi.org/10.3791/51093.

Schularick, N.M., Clark, J.J., Hansen, M.R., 2014. Primary culture of human vestibular schwannomas. J. Vis. Exp. (89). https://doi.org/10.3791/51093.

Thalmann, I., Kohut, R.I., Ryu, J., Comegys, T.H., Senarita, M., Thalmann, R., 1994. Protein profile of human perilymph: in search of markers for the diagnosis of perilymph fistula and other inner ear disease. Otolaryngol. Head Neck Surg. 111 (3P1), 273–280. https://doi.org/10.1177/01945998941113P117.

Van Abel, K.M., Carlson, M.L., Link, M.J., et al., 2013. Primary inner ear schwannomas: a case series and systematic review of the literature. Laryngoscope 123 (8), 1957–1966. https://doi.org/10.1002/lary.23928.

Xue, L., He, W., Wang, Z., Chen, H., Wang, Z., Wu, H., 2021. Characterization of a newly established schwannoma cell line from a sporadic vestibular schwannoma patient. Am. J. Transl. Res. 13 (8), 8787–8803.